Fall of a large sphere in a suspension of small fluidized particles

Ahmad Amin, Laurence Girolami, Frédéric Risso

Fall of a large sphere in a suspension of small fluidized particles

Ahmad Amin and Laurence Girolami

Laboratoire GéHCO, Campus Grandmont,

Université de Tours, 37200 Tours, France

Frédéric Risso*

Institut de Mécanique des Fluides de Toulouse, IMFT,

Université de Toulouse, CNRS - Toulouse, France

(Dated: August 13, 2022)

Abstract

The investigation of the fall of a sphere at finite Reynolds number in a concentrated suspension of small fluidized particles leads to unexpected results. By analyzing the drag force, it is shown that the average surface stress on the sphere is independent of the size of the sphere. It is proportional to an effective viscosity determined from the sedimentation velocity of the particles multiplied by the velocity of the sphere and divided by the size of the particles. These results question the role of concentration inhomogeneities that occur on a large scale in the overall flow around a moving obstacle and on a small scale near its surface.

* Corresponding author: frisso@imft.fr

Suspensions, consisting of small particles dispersed in a fluid, are very common in nature (turbidity currents, pyroclastic flows, blood, etc.) as well as in industry (food and cosmetic, fluidized beds, etc.). A suspension is a complex two-phase mixture that is desirable to model as an equivalent fluid of effective density ρ_m and viscosity μ_m. The mixture density ρ_m is simply the average density of both phases weighted by their respective volume fraction. However, defining an effective viscosity μ_m for the mixture, always larger than the suspending-fluid viscosity μ_f, remains a challenge. Since the first attempt of Einstein [1, 2], numerous works have been devoted to this issue, mainly focused on sheared suspensions of neutrally buoyant solid particles with negligible inertia. This case has been thoroughly reviewed in Ref. [3] for non-Brownian suspensions. Under these conditions, the stress τ within the mixture is linear with the shear rate $\dot{\gamma}$ and, for a given fluid-particle system, $\mu_\mathrm{m}/\mu_\mathrm{f}$ is only a function of the particle volume fraction Φ. This result may not hold with deformable particles, such as droplets in emulsions [4] or red cells in blood [5], since their deformation is affected by the shear rate $\dot{\gamma}$ and thus $\mu_\mathrm{m}/\mu_\mathrm{f}$ may depend on it. As well, when inertia is no longer negligible, $\mu_\mathrm{m}/\mu_\mathrm{f}$ may depend on the local Reynolds number and vary with $\dot{\gamma}$.

The flow around an obstacle is known as a reference case from which the rheology of a fluid can be analyzed. However, it has rarely been applied to the investigation of the effective behavior of suspensions, with the notable exception of [6], where the rise of a bubble through a dispersion of neutrally buoyant particles was studied. The present work investigates the fall of a large solid sphere through a suspension of small beads in a liquid. The beads, heavier than the liquid, are maintained in suspension by imposing a weak upward flow. Using a fluidized bed makes it possible to deal with buoyant particles and to easily control the volume fraction Φ by changing the fluidization velocity U_f. Here, U_f is taken in the range of the stable homogeneous fluidization regime, in which the particle distribution remains steady and uniform. The terminal velocity V_t of three large spheres of different diameters D is measured within four suspensions of different beads of diameters $d \ll D$, at concentrations Φ from 0.3 to 0.85. As shown later, V_t is much larger than U_f and the inertia of the suspension is not negligible as its flows around the large sphere. On the other hand, the inertia of the small beads is low compared to viscous effect.

The experimental setup is depicted in Fig. 1. The fluidization column has a rectangular cross-section of sides w_1=0.2 m and w_2=0.3 m. It is filled with a mixture of water and particles. In the absence of flow, the particles form a loose packed bed of height h_0 at

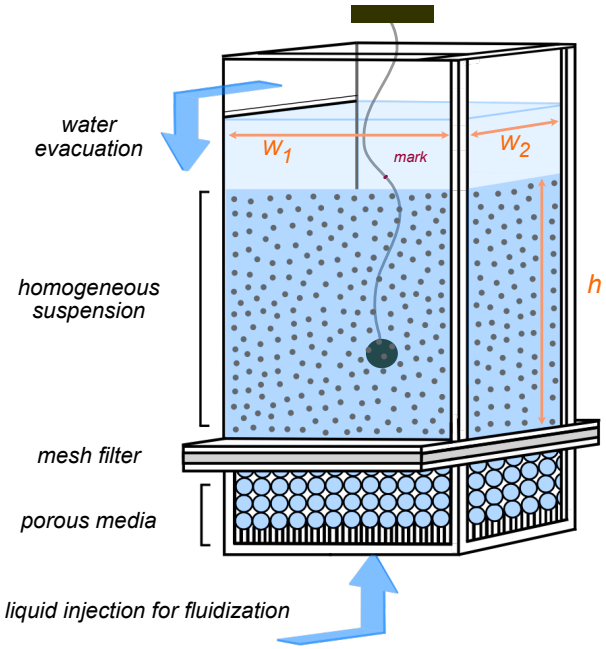

FIG. 1. Scheme of the experimental setup.

Suspension properties	GB^1	GB^2	GB^3	$Sand$
Particle diameter d [μm]	160	240	335	310
Particle density ρ_d [kg m^{-3}]	2.50×10^3	2.50×10^3	2.50×10^3	2.66×10^3
Fluid density ρ_f [kg m^{-3}]	1.0×10^3	1.0×10^3	1.0×10^3	1.0×10^3
Fluid viscosity μ_f [Pa s]	1.15×10^{-3}	1.11×10^{-3}	1.11×10^{-3}	1.10×10^{-3}
$\mathcal{S}t_0 = \frac{(\rho_\mathrm{d}-\rho_\mathrm{f})(\rho_\mathrm{d}+\frac{1}{2}\rho_\mathrm{f})gd^3}{18\ \mu_\mathrm{f}^2}$	7.6	28	76	80

TABLE I. Physical properties of the suspensions

a concentration Φ_pack between 0.58 and 0.60. Then, water is injected from the bottom at a flow rate Q through a porous media, which ensures a uniform flow, and a mesh filter, which prevents the passage of particles. For a given fluidization velocity, $U_\mathrm{f} = Q/(w_1 w_2)$, the suspension expands up to reach a height h, corresponding to a concentration $\Phi/\Phi_\mathrm{pack} = h_0/h$. The properties of the suspensions are given in Table I. We used three sets of spherical glass beads of different sizes (GB^1, GB^2, GB^3) and one set of natural sand grains. Following [10, 11], we introduce an effective viscosity of the suspension $\mu_{\mathrm{m_d}}$ determined from the fluidization velocity. Let's consider a spherical bead of diameter d and density ρ_d falling at velocity U_f into a fluid of viscosity $\mu_{\mathrm{m_d}}$ and density ρ_m. Balancing the Stokes' drag,

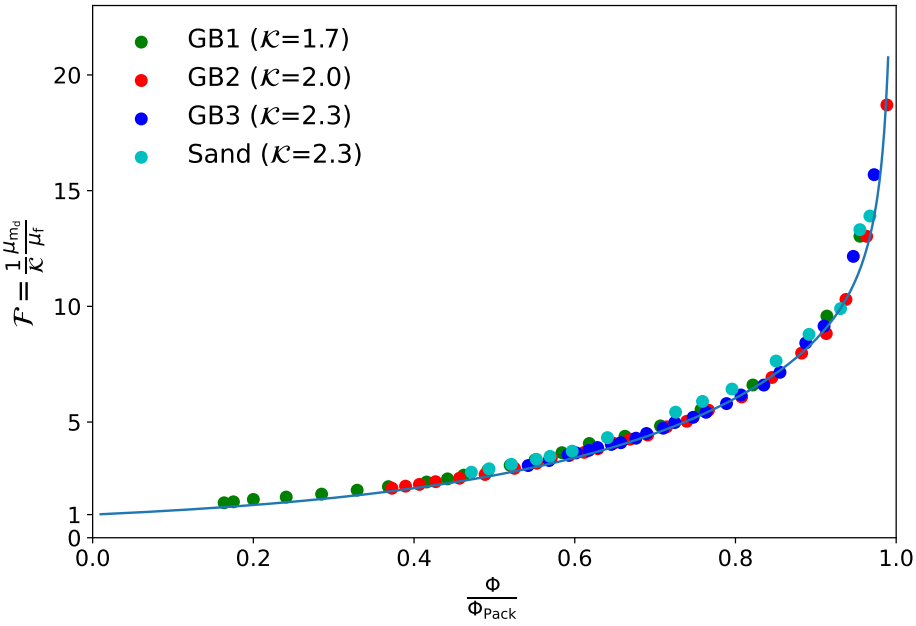

FIG. 2. Mixture effective viscosity defined from the fluidization velocity of the suspension. Symbols: measurements. Line: model from [10], taking $\mathcal{F}\left(\frac{\Phi_s}{\Phi_{\rm pack}}\right) = \frac{1}{(e^{-3}+0.08)}\left[e^{-3\left(1-\frac{\Phi_s}{\Phi_{\rm pack}}\right)} + 0.08\left(1-\frac{\Phi_s}{\Phi_{\rm pack}}\right)^{-2/3}\right]$.

$3\pi\mu_{\rm m_d} d U_{\rm f}$, by the reduced weight of the bead, $\pi d^3/6(\rho_{\rm d}-\rho_{\rm m})g$, where g is the gravity acceleration and $(\rho_{\rm d}-\rho_{\rm m}) = (1-\Phi)(\rho_{\rm d}-\rho_{\rm f})$, yields

$$\frac{\mu_{\rm m_d}}{\mu_{\rm f}} = \frac{g(\rho_{\rm d}-\rho_{\rm f})(1-\Phi)d^2}{18\mu_f U_{\rm f}}. \tag{1}$$

From the analysis of many fluid-particle systems, it has been shown in [10] that, provided that the fluid inertia is negligible, the fluidization velocity of a suspension can be modeled as

$$\frac{\mu_{\rm m_d}}{\mu_{\rm f}} = \mathcal{F}\left(\frac{\Phi}{\Phi_{\rm pack}}\right)\mathcal{K}\left(\mathcal{S}t_0\right) . \tag{2}$$

$\mathcal{F}$ is only a function of $\Phi/\Phi_{\rm pack}$, which tends towards unity as $\Phi/\Phi_{\rm pack}$ tends to zero, and towards infinity when $\Phi/\Phi_{\rm pack}$ tends to unity. $\mathcal{K}$ only depends on the Stokes number defined as $\mathcal{S}t_0 = \frac{(\rho_{\rm d}-\rho_{\rm f})(\rho_{\rm d}+\frac{1}{2}\rho_{\rm f})gd^3}{18\ \mu_{\rm f}^2}$ and accounts for the role played by the inertia of the dispersed particles through their fluctuating motion. It is constant for a given fluid-particle system and increases from 1 to 3 as $\mathcal{S}t_0$ increases from zero to infinity. Figure 2 shows that the experimental results obtained with the present suspensions collapse on the master curve proposed by [10], which validates the relevance of the viscosity $\mu_{\rm m_d}$ determined from Eq. 1.

Sphere properties	$S1$	$S2$	$S3$
Diameter D [mm]	12.2	15.7	22.4
Density ρ_{D} [kg m^{-3}]	2.64×10^3	2.60×10^3	2.50×10^3

TABLE II. Physical properties of the falling spheres

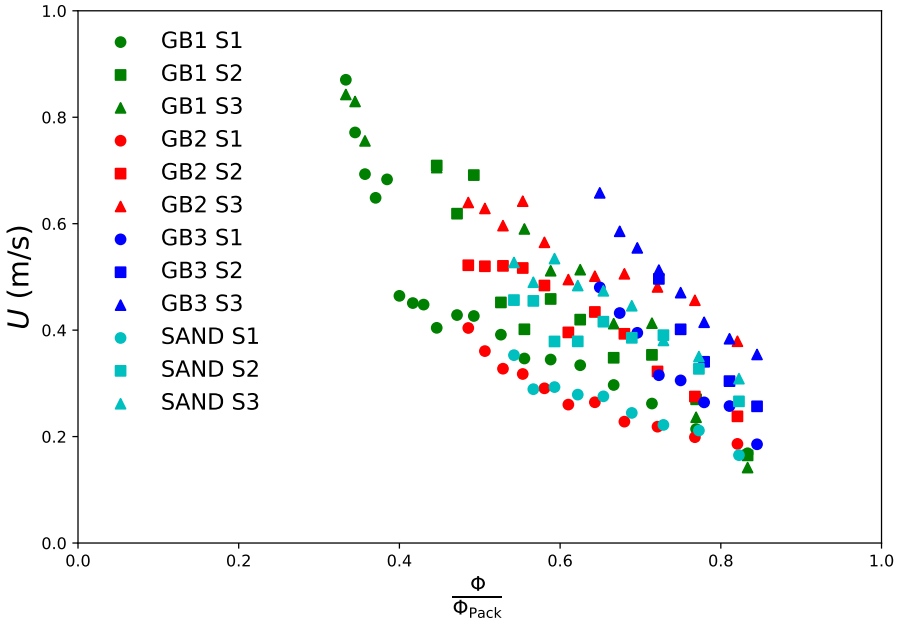

FIG. 3. Relative sphere velocity versus particle concentration.

However, $\mu_{\mathrm{m_d}}$ characterizes the viscous stresses at the scale of the dispersed beads. It is therefore not expected to be relevant to describe the macroscopic behavior of the mixture when the suspension is subjected to a shear at a scale that is large compared to d [12], as it was confirmed in [11] from comparisons with classic correlations for the effective viscosity of a sheared suspension. This motivated us to study the fall of a large sphere of diameter $D \gg d$ through such fluidized suspensions.

The characteristics of the falling spheres are given in Table II. They are made of glass and have a density close to that of the dispersed particles ($\pm 6\%$) and approximately 2.5 times that of the liquid. Their diameter ranges between 12.2 and 22.4 mm, corresponding to diameter ratios D/d from 36 to 140. The sphere falling experiments are conducted as follows. Since the suspension is opaque, we needed to find an alternative to optical methods. A thread of nylon with a diameter of 0.4 mm is attached to a support above the column, at one extremity, and glued to the sphere, at the other one. The thread length is adjusted

so that the sphere can be suspended within the column without touching the bottom. A mark is made on the thread at a location that coincides with the top of the suspension while the sphere is hanging from the support. At the beginning of a test, the sphere is fully immersed in the suspension and positioned just below the top of the fluidized bed. Then, the sphere is released and falls through the suspension until the thread is taut. A high-speed Phantom VEO 340L camera with a LED lighting is used to record the process at a rate of 1000 frames per second. The release of the sphere is visible on the movie and the end of the fall corresponds to the instant when the mark on the thread reaches the top of the bed. The uncertainties on the detection of the times of release and fall end are of ± 3 images. Depending on the system under consideration, the fall time T lies between 500 and 1300 ms and is measured with an accuracy of ± 6 ms. The fall length L is known from the thread length and varies from 20 to 60 cm, depending on the suspension height.

Because the sphere velocity $V(t)$ takes a certain time to reach its terminal value V_t, the average velocity $\langle V \rangle = L/T$ is not equal to V_t. A better approximation of V_t is obtained by assuming that the sphere motion includes a stage of constant acceleration $\dot{V}_0$ followed by a stage of constant velocity $\tilde{V}_t$. Considering that the fall length is given by $L = \int_0^T V(t)dt$, one gets that $\tilde{V}_t$ is a solution of the following second-degree equation,

$$\tilde{V}_t^2 - \left(2T\dot{V}_0\right)\tilde{V}_t + \left(2L\dot{V}_0\right) = 0\,, \tag{3}$$

the initial acceleration being obtained from the balance between the inertial forces and the reduced weight acting on the sphere,

$$\dot{V}_0 = \frac{(\rho_\mathrm{d} - \rho_\mathrm{m})g}{\rho_\mathrm{d} + \frac{1}{2}\rho_\mathrm{m}}\,, \tag{4}$$

where $\frac{1}{2}\rho_\mathrm{m}$ accounts for the added mass. With this model, the terminal velocity is reached at time $t_\mathrm{t} = \tilde{V}_\mathrm{t}/\dot{V}_0$. Thus $\tilde{V}_\mathrm{t}$ tends towards V_t when t_t/T becomes small, i.e. when the acceleration stage is short compared to the whole fall duration. We have determined $\langle V \rangle$, $\tilde{V}_\mathrm{t}$ and t_t/T for all the tests made. In the following, only the tests with $t_\mathrm{t}/T \leq 0.3$ have been retained. In this case, the difference between $\langle V \rangle$ and $\tilde{V}_t$ is less than 15% and we estimate that the discrepancy between $\tilde{V}_\mathrm{t}$ and V_t is less than 5%. All the subsequent analysis is thus done by using $\tilde{V}_\mathrm{t}$ as the terminal velocity of the spheres. Note that the experimental data have also been processed by considering a less demanding criterion $t_\mathrm{t}/T \leq 0.5$, which does not change the present conclusions and proves the robustness of the results regarding the determination of $\tilde{V}_\mathrm{t}$.

The terminal velocity U of the sphere relative to the fluid-particle mixture is obtained by adding the fluidization velocity U_f, so that $U = V_\mathrm{t} + U_\mathrm{f}$. Figure 3 shows U as a function of Φ/Φ_pack for the three spheres and the four types of suspensions. The values of U ranges between 0.1 and 0.9 m/s and are much larger than the fluidization velocities, which remain less than 0.01 m/s. In any case, U is thus almost equal to V_t. It is a decreasing function of Φ/Φ_pack, since both the density and the effective viscosity of the suspension increase with the solid volume fraction. For a given type of bead, U is also observed to decrease with D. However, it is difficult to draw physical conclusions from these dimensional plots.

As shown by [6], an important dimensionless group is the other Stokes number defined by $St = \tau_d/\tau_D$, which compares the response time of the dispersed particles, $\tau_d = (\rho_\mathrm{d} + \frac{1}{2}\rho_\mathrm{m})d^2/18\mu_{\mathrm{m_d}}$, to the time scale of the flow generated by the motion of the large body, $\tau_D = D/U$. For $St < 1$, the particles are expected to follow the stream lines of the suspending fluid, whereas, for $St > 1$, they may collide with the large body. In the present case, this Stokes number is much less than unity ($2 \times 10^{-3} < St < 9 \times 10^{-2}$). However, this analysis is not sufficient to conclude that the suspension remains homogeneous. First, shear-rate gradients in the flow around the sphere may induce particle migration [7], leading to non-uniform concentration. In addition, a depletion of particles in the wake behind the obstacle have been reported in previous studies [8, 9].

Now, the results are analyzed in terms of the relationship between the drag coefficient and the Reynolds number of the falling sphere. If the drag coefficient is obtained directly from the balance between the drag force and the reduced weight of the sphere, $C_\mathrm{d} = \frac{4}{3}\frac{(\rho_\mathrm{D}-\rho_\mathrm{m})gD}{\rho_\mathrm{m}U^2}$, the Reynolds number requires the knowledge of the effective viscosity of the suspension. Let us consider the viscosity $\mu_{\mathrm{m_d}}$ defined by Eq. 1 and introduce $Re_\mathrm{m} = \frac{\rho_\mathrm{m}UD}{\mu_{\mathrm{m_d}}}$. Figure. 4 shows log-log plots of the experimental values of C_d versus Re_m, for all investigated cases. For any given pair of sphere and suspension, the values of C_d collapse on a ${Re_\mathrm{m}}^{-1}$ straight line. On these plots, the Reynolds number has been divided by a constant k, which has been arbitrarily adjusted to make the data of the various systems to coincide with the drag Stokes law, $C_\mathrm{d} = 24/Re$. The values of k varies from one system to another, but remain constant for a given system, which means that they are independent of Re_m. In Fig. 5, k is plotted against D/d and turns out to be a linear function of the sphere-to-bead diameter ratio: $k = \alpha D/d$, with $\alpha \approx 0.58$. Therefore, the experimental results lead to the following

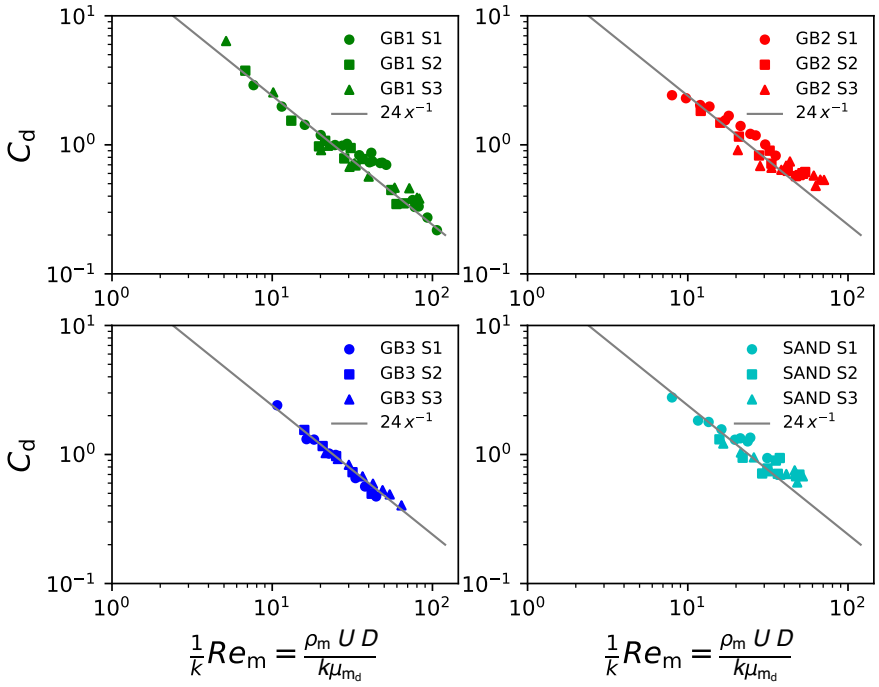

FIG. 4. Drag coefficient of the sphere versus the Reynolds number (values of k in Fig 5).

quite unexpected expressions of the drag coefficient,

$$C_{\mathrm{d}} = 24\,\frac{\mu_{\mathrm{m_d}}}{\rho_m U D}\,\alpha\frac{D}{d} = 24\alpha\,\frac{\mu_{\mathrm{m_d}}}{\rho_m U d}\,, \tag{5}$$

and the drag force

$$F_{\mathrm{D}} = (\pi D^2)\,\mu_{\mathrm{m_d}}\frac{3\alpha U}{d}\,. \tag{6}$$

Thus it turns out that the drag coefficient C_{d}, as well as the average stress on the sphere surface $\tau_{\mathrm{p}} = F_{\mathrm{D}}/\pi D^2 = (3\alpha)\,\mu_{\mathrm{m_d}}\frac{U}{d}$, are independent of the size D of the falling sphere and proportional to $\mu_{\mathrm{m_d}}$.

We now discuss possible interpretations of this surprising result. A first naive approach is to assume that the suspension remains homogeneous and that its behavior is controlled by an effective viscosity μ_{m} that is constant throughout the flow. By equating Eq. 6 to the Stokes' drag,

$$F_{\mathrm{D_{St}}} = (\pi D^2)\,\mu_{\mathrm{m}}\frac{3U}{D}\,, \tag{7}$$

one finds

$$\mu_{\mathrm{m}} = \alpha\mu_{\mathrm{m_d}}\frac{D}{d}\,. \tag{8}$$

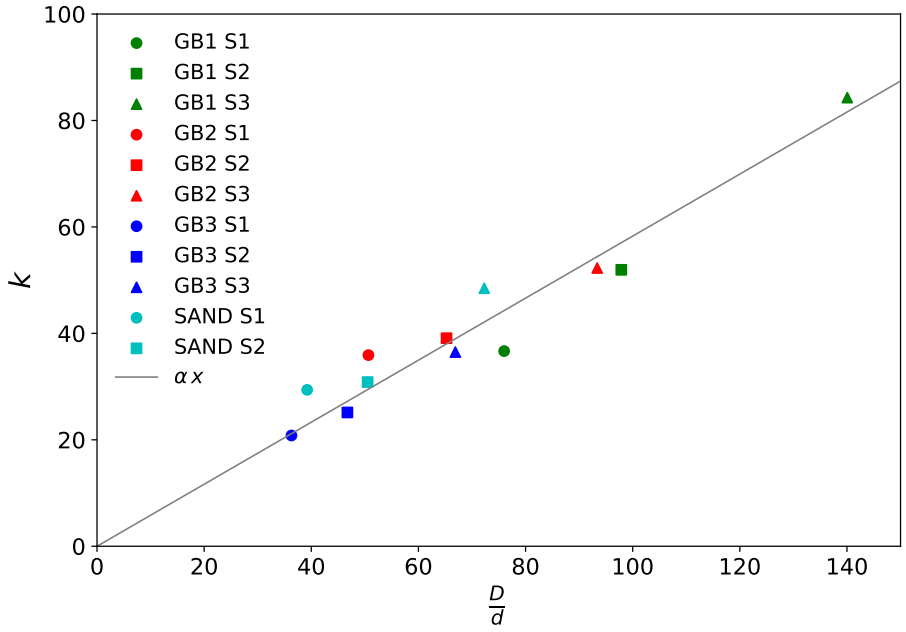

FIG. 5. Coefficient k against $\frac{D}{d}$.

However, this expression is inconsistent. As $\mu_{\mathrm{m_d}}$ represents the effective viscosity at the scale d of the beads, one could expect the effective viscosity at a much larger scale D to be different, but converge towards a constant values at large D/d, which is not the case here. Otherwise, one can assume that μ_{m} actually varies with D because it would depend on the shear rate $\dot{\gamma} \propto U/D$, but that leads to contradictory behaviors according to that $\dot{\gamma}$ varies by changing either U or D. Moreover, the sphere Reynolds number based on μ_{m} is too large ($5 < \rho_{\mathrm{m}} U D/\mu_{\mathrm{m}} < 100$, see Fig. 4) for the Stokes' drag law to be valid. Therefore, the effective viscosity of the suspension cannot be determined from Eq. 8.

As noted by [13], determining the effective viscosity of a suspension from the measurement of the force exerted on a wall requires the homogeneity of the suspension everywhere, and in particular near the wall. The present result is probably associated with the fact that the particle concentration is not uniform. We think that it is relevant to discuss separately the effect of inhomogeneity at the scale D of the flow around the large sphere and that of inhomogeneity at the scale d of the dispersed particles. Regarding large scales, the expected increase of the particle concentration at the sphere front and the decrease at its rear can significantly influence the drag coefficient [8, 9] and eventually lead to unexpected behaviors. In our opinion, such a mechanism can hardly result in a drag coefficient that both decreases

as the reciprocal of the velocity and does not depend on D. However, due to the complexity of such flows, the question of its relevance remains open.

At the scale of the particles, the homogeneity of the suspension is never rigorously fulfilled in the vicinity of a solid surface. Since a particle cannot approach an obsctacle at a distance that is closer than its radius, the volume fraction of the dispersed phase tends to zero at a solid surface [14, 15]. In addition, the interactions between a solid surface and the dispersed particles differ from the interactions between a solid surface and the suspending fluid. A fluid adheres to a solid because of molecular interactions such as van der Waals forces, whereas dispersed particles can move relative to a solid. Considering the blood flow for example, the red blood cells may experience a slip velocity of 40% of the maximum flow velocity relative to the vessel wall [16]. In the framework of two-fluid approaches, this can be modeled by increasing the viscosity of the plasma near the vessel wall in order to account for the additional dissipation induced by the slip motion of the cells [17]. However, it is not relevant to model the whole mixture as a homogeneous fluid satisfying a non-slip condition at a solid boundary. This suggests another possible interpretation of the experimental result. We can assume that there is a thin layer of liquid at the surface of the sphere of thickness δ which is devoid of particles, and that the particles just outside this layer move at a speed of the order of U with respect to the surface of the sphere. Within this layer, the liquid is submitted to a stress $\tau_p \approx \mu_\mathrm{f} \frac{U}{\delta}$. As $\mu_\mathrm{md} \frac{U_\mathrm{f}}{d}$ is the average stress submitted by the liquid passing through the fluidized particles, it seems relevant to assume that $\tau_p \approx \mu_\mathrm{md} \frac{U}{d}$, which corresponds to the experimental result. By considering that the flow in the near vicinity of the sphere surface is independent of the large-scale flow around the sphere, this interpretation is naturally consistent with the fact the drag coefficient is proportional to U^{-1} and independent of D.

Apart from the blood circulation, a few other studies of dispersed two-phase flows have reported evidences of such a slip of the dispersed phase near a solid surface. A foam in a pipe was shown to behave as a rigid body slipping on a lubricated layer at the wall and the authors concluded that "the flow of such foams is not controlled by foam rheology" [18]. The flow of a concentrated gas-solid suspension released after a dam break was also observed to flow as an inviscid fluid which slips on the wall [19]. Regarding an imposed wall shear rate, it is worth mentioning an investigation of the flow of a homogeneous oil-in-water droplet emulsion in a pipe [4]. While the effective viscosity of the emulsion μ_m was found to vary over the pipe cross-section and to depend on the bulk velocity U, the viscosity at the

wall $\mu_{\mathrm{m_w}}$ was observed to be independent of U and the pressure drop along the pipe to be proportional to $\mu_{\mathrm{m_w}}U$. This surprising outcome is fully compatible with the present result, $\tau_p = \mu_{\mathrm{m_d}} \frac{3\alpha U}{d}$, where $\mu_{\mathrm{m_d}}$ is independent of U and implies a pressure drop that is proportional to $\mu_{\mathrm{m_d}}U$, whatever the nature of the flow or the mixture rheology away from the wall.

To conclude, the fall of a large sphere in a fluidized suspension of small particles has been investigated in the regime where the flow inertia is negligible at the scale of the particle but not at that of the sphere. The drag force (Eq. 6) is found to be the product of the sphere area πD^2, the viscosity μ_{m_d} determined from the fluidization velocity of the dispersed particles (Eq. 1), and the ratio U/d of the sphere velocity and the particle diameter. The fact that the drag coefficient depends on the Reynolds number based on the diameter of the dispersed particles rather than that of the falling sphere is quite unexpected. It is likely associated with the fact that the suspension does not remain homogeneous. Two interpretations, based on either a large-scale inhomogeneity or a particle slip velocity at the sphere surface, have been discussed. They are not mutually exclusive. Indeed, the stress along the sphere surface is probably not constant. The most likely situation is that the stress near the front stagnation point is mainly normal and rather scales as U/D, and that the pressure difference between the front and the rear of the sphere are mainly controlled by the large-scale inhomogeneity. On the other hand, the shear rate near the equator probably scales as $\tau_p \approx \mu_{\mathrm{f}} \frac{U}{\delta}$ with $\delta \ll d$. We are inclined to think that the magnitude of the latter may be much larger than the former, so that its contribution dominates the overall friction. However, since the local particle concentration and velocity have not been measured, no definitive conclusions regarding the physical mechanism can be reached. Future numerical works should determine whether a large-scale inhomogeneity may be consistent with the present experimental scaling and future experimental works should assess the existence of a strong slip velocity at the sphere surface.

---

[1] A. Einstein, Eine neue Bestimmung der Moleküldimensionen, Ann. Phys. **19**, 289 (1906).

[2] A. Einstein, Berichtigung zu meiner Arbeit: Eine neue Bestimmung der Moleküldimensionen, Ann. Phys. **34**, 591 (1911).

[3] É Guazzelli and O. Pouliquen, Rheology of dense granular suspensions, J. Fluid Mech. **852**,

P1 (2018).

[4] M. Abbas, M., A. Pouplin, O. Masbernat, A. Liné and S. Décarre, Pipe flow of a dense emulsion: Homogeneous shear-thinning or shear-induced migration?, AIChE J. **63**, 5182 (2017).

[5] A. S. Popel and P. C. Johnson, Microcirculation and hemology, Annu. Rev. Fluid Mech. **37**, 43 (2005).

[6] N. Hooshyar, van J. R. Ommen, P. J. Hamersma, S. Sundaresan and R. F. Mudde, Dynamics of single rising bubbles in neutrally buoyant liquid-solid suspensions, Phys. Rev. Lett. **110**, 244501 (2013).

[7] D. Leighton and A. Acrivos, The shear-induced migration of particles in concentrated suspensions, J. Fluid Mech. **181**, 415 (1987).

[8] H. Haddadi, S. Shojaei-Zadeh and J. F. Morris, Lattice-Boltzmann simulation of inertial particle-laden flow around an obstacle, Phys. Rev. Fluids **1**, 024201 (2016).

[9] T. Dbouk, A suspension balance direct-forcing immersed boundary model for wet granular flows over obstacles, J. Non-Newtonian Fluid Mech. **230**, 68 (2016).

[10] A. Amin, L. Girolami and F. Risso, On the fluidization/sedimentation velocity of a homogeneous suspension in a low-inertia fluid, Powder Tech. **391**, 1 (2021).

[11] L. Girolami and F. Risso, Sedimentation of gas-fluidized particles with random shape and size, Phys. Rev. Fluids **4**, 074301 (2019).

[12] E. J. Hinch, An averaged-equation approach to particle interactions in a fluid suspension, J. Fluid Mech. **83**, 695 (1977).

[13] G. Ovarlez, F. Bertrand and S. Rodts, Local determination of the constitutive law of a dense suspension of noncolloidal particles through magnetic resonance imaging, J. Rheol. **50**, 259 (2006).

[14] N. Lubchenko, B. Magolan, R. Sugrue, E. Baglietto, A more fundamental wall lubrication force from turbulent dispersion regularization for multiphase CFD applications, Int. J. Multiphase Flow. **98**, 36 (2018).

[15] A. du Cluzeau, G. Bois and A. Toutant, Analysis and modelling of Reynolds stresses in turbulent bubbly up-flows from direct numerical simulations, J. Fluid Mech. **866**, 132 (2019).

[16] S. Roman, S. Lorthois, P. Duru and F. Risso, Velocimetry of red blood cells in microvessels by the dual-slit method: Effect of velocity gradients, Microvasc. Res. **84**, 249 (2012).

[17] M. Sharan and A. S. Popel, A two-phase model for flow of blood in narrow tubes with increased

effective viscosity near the wall, Biorheology **38**, 415 (2001).

[18] M. I. Briceño and D. D. Joseph, Self-lubricated transport of aqueous foams in horizontal conduits, Int. J. Multiphase Flow **29**, 1817 (2003).

[19] L. Girolami and F. Risso, Physical modeling of the dam-break flow of sedimenting suspensions, Phys. Rev. Fluids **5**, 084306 (2020).